

Ancient Igneous Intrusions and Early Expansion of the Moon Revealed by GRAIL Gravity Gradiometry

Jeffrey C. Andrews-Hanna,^{1*} Sami W. Asmar,² James W. Head III,³ Walter S. Kiefer,⁴ Alexander S. Konopliv,² Frank G. Lemoine,⁵ Isamu Matsuyama,⁶ Erwan Mazarico,^{5,7} Patrick J. McGovern,⁴ H. Jay Melosh,⁸ Gregory A. Neumann,⁵ Francis Nimmo,⁹ Roger J. Phillips,¹⁰ David E. Smith,⁷ Sean C. Solomon,^{11,12} G. Jeffrey Taylor,¹³ Mark A. Wieczorek,¹⁴ James G. Williams,² Maria T. Zuber⁷

¹Department of Geophysics and Center for Space Resources, Colorado School of Mines, Golden, CO 80401, USA. ²Jet Propulsion Laboratory, Pasadena, CA 91109, USA. ³Department of Geological Sciences, Brown University, Providence, RI 02912, USA. ⁴Lunar and Planetary Institute, Houston, TX 77058, USA. ⁵Solar System Exploration Division, NASA Goddard Space Flight Center, Greenbelt, MD 20771, USA. ⁶Lunar and Planetary Laboratory, University of Arizona, Tucson, AZ 85721, USA. ⁷Department of Earth, Atmospheric and Planetary Sciences, Massachusetts Institute of Technology, Cambridge, MA 02139-4307, USA. ⁸Department of Earth and Atmospheric Sciences, Purdue University, West Lafayette, IN 47907, USA. ⁹Department of Earth and Planetary Sciences, University of California, Santa Cruz, Santa Cruz, CA 95064, USA. ¹⁰Planetary Science Directorate, Southwest Research Institute, Boulder, CO 80302, USA. ¹¹Department of Terrestrial Magnetism, Carnegie Institution of Washington, Washington, DC 20015, USA. ¹²Lamont-Doherty Earth Observatory, Columbia University, Palisades, NY 10964, USA. ¹³Hawaii Institute of Geophysics and Planetology, University of Hawaii, Honolulu, HI 96822, USA. ¹⁴Institut de Physique du Globe de Paris, Univ. Paris Diderot, 75205 Paris Cedex 13, France.

*To whom correspondence should be addressed. E-mail: jcahanna@mines.edu

The earliest history of the Moon is poorly preserved in the surface geologic record because of the high flux of impactors, but aspects of that history may be preserved in subsurface structures. Application of gravity gradiometry to observations by the Gravity Recovery and Interior Laboratory mission results in the identification of a population of linear gravity anomalies with lengths of hundreds of kilometers. Inversion of the gravity anomalies indicates elongated positive density anomalies interpreted to be ancient vertical tabular intrusions or dikes, formed by magmatism in combination with extension of the lithosphere. Crosscutting relationships support a pre-Nectarian to Nectarian age, preceding the end of the heavy bombardment of the Moon. The distribution, orientation, and dimensions of the intrusions indicate a globally isotropic extensional stress state arising from an increase in the Moon's radius by 0.6-4.9 km early in lunar history, consistent with predictions of thermal models.

Planetary gravity analyses have been limited historically to large-scale features associated with high contrasts in density, because of the low resolution and low signal-to-noise ratio of the data. As a result, small-scale subsurface structures such as faults and dikes that have been inferred from their surface expressions have not been resolved in the gravity field, and structures lacking a direct surface manifestation have been largely undocumented. This situation has posed a challenge for studies of the early evolution of the Moon because the near saturation of the surface by impact craters has erased much of the geological record from the first ~700 million years (Myr) of lunar history (1), spanning the critical period of time between the solidification of the lunar magma ocean and the end of major impact basin formation ~3.8 billion years ago (Ga) (2). Data from the Gravity Recovery and Interior Laboratory (GRAIL) mission (3) now permit the expansion of the gravity field to spherical harmonic degree and order 420 (model GL0420A), corresponding to a half-wavelength resolution of ~13 km at the lunar surface (4). This resolution is sufficient to resolve short-wavelength density anomalies such as

intrusions having a higher density than the surrounding rocks and faults that offset layers of differing density.

Here we apply the technique of gravity gradiometry to the GRAIL gravity field, using the second spatial derivatives of the gravitational potential to highlight short-wavelength features associated with discrete structures (5). In terrestrial applications, gradients are typically measured directly by a three-axis gradiometer on an aerial or satellite-borne platform (5, 6), but here the gradients were calculated from the potential field. In order to emphasize subsurface structures, we used gradients of the Bouguer potential (calculated as the difference between the measured gravitational potential and the potential arising from the effects of topography) (4). The maximum amplitude of the second horizontal derivative of the Bouguer potential at each point on the surface [Γ_{hh} , measured in Eötvös, where $1E = 10^{-9} \text{ s}^{-2}$; (7)] was then calculated. The resulting horizontal Bouguer gradient map (Fig. 1) displays a rich array of short-wavelength structures in the lunar crust.

The dominant features in the gradient map are the ring structures surrounding the large impact basins. These rings are also observed in the Bouguer gravity (Fig. 1A) (4), but they are resolved in the gradient map as discrete structures. Outside of the basins, a large number of irregular small-scale anomalies are observed with typical values of $\pm 10E$, likely arising from small-scale density anomalies in the upper crust associated with variations in composition or porosity. In addition, a number of elongated linear gravity anomalies (LGAs) characterized by negative gradients stand out clearly above the background variability.

Four of the LGAs have lengths exceeding 500 km (Fig. 2). These anomalies closely follow linear paths (great circles) across the surface, to within root mean square (RMS) deviations of 1-3% of their lengths. Inspection of the most distinct LGAs yields 22 probable anomalies with a combined length of 5300 km, and an additional 44 possible anomalies with a combined length of 8160 km, for a total length of 13,460 km (Fig. 1C). An independent automated algorithm identified 46 anomalies with a combined length of 10,600 km (7). Such remarkably linear structures in natural geologic systems are typically associated with faults or dikes. Averaged profiles of the Bouguer gravity anomaly perpendicular to the lineations show them to be associated with narrow positive gravity anomalies (Fig. 3), indicating subsurface structures of increased density consistent with the interpretation that the features are mafic igneous intrusions.

We used a Monte Carlo approach to invert the average Bouguer gravity profiles across the LGAs for the physical properties of the subsurface density anomalies, treating them as tabular bodies of unknown

top depth, bottom depth, width, and density contrast (7). A continuous set of solutions exists with comparable misfits to the data, as a result of the fundamental non-uniqueness of potential field data with respect to subsurface structures. The 95% confidence intervals of the model parameters were also determined from the variability in the gravity profiles. For one of the best-defined anomalies (LGA-1, Fig. 2A), the best-fit solutions have density contrasts of 160-960 kg m⁻³ in bodies with widths of 5-25 km extending between a top depth of 10-15 km and a bottom depth of 76-91 km (Fig. 3 and Table 1). The top depth may correspond either to the top of the intrusion or to the maximum depth of impact brecciation and gardening, above which the density contrast would become less distinct. Similarly, the bottom depth may correspond either to the base of the intrusion or to the depth of the crust-mantle interface, below which the density contrast between the intrusion and the host rocks would decrease markedly. For LGA-2, a shallow top depth is suggested by the observation that the 116-km-diameter impact crater Roche, excavating the crust to a depth of ~7 km and brecciating it to greater depths, results in a modest reduction in the magnitude of the anomaly, whereas smaller craters have no effect (Fig. 2).

The dimensions of the anomaly sources can be further constrained using independent constraints on the density contrast. The mean density of the upper crust derived from GRAIL is 2550 ± 250 kg m⁻³ (8). Although the composition of the intrusions is unknown, representative values can be taken from the measured densities of lunar igneous rocks of 3100-3350 kg m⁻³ (9), yielding density contrasts of 550-860 kg m⁻³. For density contrasts of 550 and 800 kg m⁻³, the best-fit solutions for LGA-1 collapse to a point in parameter space, with widths of 7.6 and 5.3 km, respectively (Table 1). However, the bottom depth for these solutions of 85-86 km is likely deeper than the base of the crust, below which the reduced density contrast would contribute little to the observed gravity. If the base of the density anomaly is constrained to be 40 km, comparable to the mean crustal thickness (8), the best-fit widths for density contrasts of 550 and 800 kg m⁻³ increase to 29.1 and 23.5 km, with top depths of 24.9 and 26.9 km. A bottom depth of 60 km results in widths of 11.9 and 8.3 km, and top depths of 19.0 and 19.4 km. Similar results are found from the inversions of LGAs 2 and 4, with a total range of best-fit widths of 5-12 km for density contrasts of 550 and 800 kg m⁻³ with the bottom depth unconstrained, or 7-41 km for bottom depths of 40-60 km (7). LGA-3 requires a greater width of 13-18 km, or 49-82 km with the bottom depth constrained to 40-60 km, in keeping with the greater width of the gravity anomaly.

Although the lengths and linearity of the density anomalies are similar to those of giant dike swarms on Earth, Mars, and Venus, their widths greatly exceed typical dike widths of tens of meters (10, 11). Vertical tabular intrusions with aspect ratios similar to those proposed here can form by diapirism when the viscosity contrast between the magma and host rock is in the range of 10⁶-10⁸ (12). For mafic intrusions, this low viscosity contrast would require either a partially crystalline intrusion, or a highly ductile or partially molten host rock. The source of the gravity anomalies may be analogous to the Great Dyke of Zimbabwe, which likely formed as a result of shallow intrusive activity during ancient rifting (13). This elongated layered ultramafic intrusion measures 550 km in length, 3-11 km in width, and up to 12 km in vertical extent (13, 14). Intrusive bodies of similar scale have been inferred to exist beneath the Valles Marineris region of Mars on the basis of collapse features (15), formed in response to lithospheric extension and intrusion (16). Alternatively, narrow swarms of closely spaced dikes (17) can match the gravity anomalies but would require tens to hundreds of dikes confined within zones less than ~40 km wide that extend over distances of hundreds of kilometers. Similar narrow dike swarms with lengths up to 100 km form above elongated axial magma chambers in rifts on Earth (18). A combination of the above processes may be responsible for the anomalies, with a single vertical tabular intrusion forming in a partially

molten lower crust, sourcing a swarm of closely spaced dikes in the more brittle upper crust. The large bottom depths from the inversions permit the intrusions to extend into the mantle, as would be required if the rise of magma were governed by neutral buoyancy (19). Although the specific nature and formation mechanism of the intrusions remains uncertain, some form of intrusive activity in a horizontally extensional stress regime is indicated by all of the analogous structures.

Lunar dikes previously inferred from geological analyses (20) are not detected in the gravity data. This result is not surprising, because isolated dikes with widths of up to tens of meters would have gravity anomalies two orders of magnitude smaller than these LGAs. A linear magnetic anomaly interpreted as a dense swarm of dikes on the floor of the South Pole-Aitken basin (17) is not evident in the gravity gradients, but is associated with a broad positive Bouguer gravity anomaly where it extends outside of the basin (7). This anomaly may be consistent with a dense dike swarm, with the lower density contrast relative to the mafic crust in the floor of the basin possibly accounting for the non-detection there. Alternatively, the poor expression of the magnetic anomalies in the gravity data may support Fe-rich material derived from the basin-forming projectile as the source of the magnetic anomalies (21).

Averaged magnetic (22) and topographic (23) profiles across the LGAs generally reveal no correlation of either dataset with the gravity anomalies (7). Forward models of the expected magnetic anomalies require that any magnetization be substantially less than 0.1 A/m for most of the lineations, indicating that the intrusions either have very low magnetic susceptibility or cooled in the absence of an external field. A topographic signature associated with the intrusions might be expected as a result of tectonic uplift, flexural subsidence, graben formation (24), or collapse of the surface into the magma chambers (15), yet none is observed. A number of LGAs are located in crater-saturated areas (Fig. 2) and lack any obvious surface expression in topography, image, or other remote sensing datasets. The absence of a surface expression is consistent with an age for the structures that predates the superimposed crater population and the surface geologic record.

The age of the structures can be further constrained by crosscutting relationships. Several linear anomalies are observed radial to the South Pole-Aitken impact basin, which is the oldest basin on the Moon. This radial orientation indicates that the formation of these structures was influenced by the pre-existing basin. The lack of a surface signature rules out an origin as rays of dense impact ejecta (7). A 1000-km-long anomaly (LGA-4) crosses the Crisium basin at an oblique angle (Fig. 2), but no trace of the anomaly is found within the basin itself. This geometry suggests that this anomaly predated Crisium and that the underlying structure was destroyed within the basin cavity by the impact. This timing is supported by the fact that intrusion is not deflected by the strong flexural stresses associated with the pre-mare mascon (25) and later mare load within the basin. By these arguments, the South Pole-Aitken and Crisium basins bracket the formation of the largest intrusions to be in the pre-Nectarian to early Nectarian time frame, prior to the end of the basin-forming epoch at ~3.8 Ga. This age is consistent with the lunar intrusive activity between 4.2 and 4.5 Ga responsible for the formation of the plutonic Mg-suite rocks (26), though it is not possible to directly link these intrusions to any particular rock type using gravity data alone.

Tabular igneous intrusions form perpendicular to the most extensional principal stress direction (27), leading to the formation of vertical dikes in a horizontally extensional stress field and sills in a horizontally compressional stress field. Although local flexural stresses or structural control can alter the orientation of intrusions (7), the LGAs are distributed uniformly across the Moon and show no clear preferred orientations or association with known flexurally supported loads. This pattern indicates largely isotropic horizontal extension as would be expected to arise from global expansion. However, the lunar lithosphere is thought to have been in a state of compression throughout most of its history as a result

of interior cooling and global contraction (28). Superimposed stresses associated with the outward migration of the Moon, with or without contemporaneous true polar wander, are similarly inconsistent with the locations and orientations of the LGAs (7, 29). At the time of the intrusive activity inferred here, the lithosphere must have been in a horizontally extensional stress state in order to accommodate the inflation of the vertical tabular intrusions. Taking the total length of the probable intrusion population of 5300 km and the typical best-fit widths of 5–40 km, the resulting horizontal extensional strain of 0.035–0.27% equates to an increase in the lunar radius by 0.6–4.8 km. However, this estimate is complicated by the possibility of viscous accommodation of some of the growth of the intrusions, or lithospheric extension not accompanied by intrusive activity that would go undetected by GRAIL.

Such a period of early extension was predicted by some thermal history models (28), developed to account for the absence of a global population of large thrust faults on the Moon similar to those found on Mercury. The thermal models best matched that constraint with an initial condition that included a 200–300-km-deep magma ocean and a cooler deep interior, leading to coupled warming of the interior and cooling of the outer shell, with net expansion in the first billion years followed by modest global contraction. Cooling and contraction of the lunar lithosphere could also have contributed to extensional strain at the depths of these intrusions within the first few tens of millions of years after lunar crustal formation. This thermal inversion may be a natural outcome of the post-accretionary temperature profile of the Moon (30). Thermal history models that satisfy the constraint of <1 km decrease in radius over the last 3.8 Ga also predict 2.7–3.7 km of global expansion during the first ~1 Ga, with the highest rates occurring during the first 0.5 Ga (28), consistent with our proposed period of expansion. The amount of predicted expansion is sensitive to the depth of the magma ocean and the initial temperature of the deep interior. However, no direct geological evidence for this early expansion has previously been found, as a consequence of the intense cratering of the surface at that time. This earliest epoch of lunar expansion is now revealed by GRAIL gravity data, which sees through the surface geology to the hidden structures beneath. This result places a constraint on lunar evolution and raises important questions regarding the early evolution of other terrestrial planets, because the first ~700 Myr of planetary evolution is poorly preserved in the geological records of all of the planets.

References and Notes

- W. K. Hartmann, R. W. Gaskell, Planetary cratering 2: Studies of saturation equilibrium. *Meteoritics* **32**, 109 (1997). doi:10.1111/j.1945-5100.1997.tb01246.x
- D. Stöffler, G. Ryder, Stratigraphy and isotope ages of lunar geologic units: Chronological standard for the inner solar system. *Space Sci. Rev.* **96**, 9 (2001). doi:10.1023/A:1011937020193
- M. T. Zuber *et al.*, Gravity Recovery and Interior Laboratory (GRAIL): Mapping the lunar interior from crust to core. *Space Sci. Rev.* **10**.1007/s11214-012-9952-7 (2012).
- M. T. Zuber *et al.*, Gravity field of the Moon from the Gravity Recovery and Interior Laboratory (GRAIL) mission. *Science* **10.1126/science.1231507** (2012).
- C. Jekeli, Airborne gradiometry error analysis. *Surv. Geophys.* **27**, 257 (2006). doi:10.1007/s10712-005-3826-4
- R. Rummel, W. Yi, C. Stummer, GOCE gravitational gradiometry. *J. Geod.* **85**, 777 (2011). doi:10.1007/s00190-011-0500-0
- Materials and methods are available as supplementary materials on Science Online.
- M. A. Wieczorek *et al.*, The crust of the Moon as seen by GRAIL. *Science* **10.1126/science.1231530** (2012).
- W. S. Kiefer, R. J. Macke, D. T. Britt, A. J. Irving, G. J. Consolmagno, The density and porosity of lunar rocks. *Geophys. Res. Lett.* **39**, L07201 (2012). doi:10.1029/2012GL051319
- R. E. Ernst, E. B. Grosfils, D. Mège, Giant dike swarms: Earth, Venus, and Mars. *Annu. Rev. Earth Planet. Sci.* **29**, 489 (2001). doi:10.1146/annurev.earth.29.1.489
- L. Wilson, J. W. Head III, Lunar volcanism: Factors controlling intrusion geometries and eruption conditions. *Lunar Planet. Sci.* **40**, abstract 1160 (2009).
- A. M. Rubin, Dikes vs. diapirs in viscoelastic rock. *Earth Planet. Sci. Lett.* **119**, 641 (1993). doi:10.1016/0012-821X(93)90069-L
- A. H. Wilson, The geology of the Great “Dyke,” Zimbabwe: The ultramafic rocks. *J. Petrol.* **23**, 240 (1982). doi:10.1093/petrology/23.2.240
- F. Podmore, A. H. Wilson, A reappraisal of the structure and emplacement of the Great Dyke, Zimbabwe. *Geol. Assoc. Canada Special Paper* **33**, 317 (1985).
- D. Mège, A. C. Cook, E. Garel, Y. Lagabrielle, M. Cormier, Volcanic rifting at martian grabens. *J. Geophys. Res.* **108**, 5044 (2003). doi:10.1029/2002JE001852
- J. C. Andrews-Hanna, The formation of Valles Marineris: 2. Stress focusing along the buried dichotomy boundary. *J. Geophys. Res.* **117**, E04009 (2012). doi:10.1029/2011JE003954
- M. E. Purucker, J. W. Head III, L. Wilson, Magnetic signature of the lunar South Pole-Aitken basin: Character, origin, and age. *J. Geophys. Res.* **117**, E05001 (2012). doi:10.1029/2011JE003922
- A. Gudmundsson, Infrastructure and mechanics of volcanic systems in Iceland. *J. Volcanol. Geotherm. Res.* **64**, 1 (1995). doi:10.1016/0377-0273(95)92782-Q
- J. W. Head III, L. Wilson, Absence of large shield volcanoes and calderas on the Moon: Consequence of magma transport phenomena? *Geophys. Res. Lett.* **18**, 2121 (1991). doi:10.1029/91GL02536
- J. W. Head III, L. Wilson, Lunar graben formation due to near-surface deformation accompanying dike emplacement. *Planet. Space Sci.* **41**, 719 (1993). doi:10.1016/0032-0633(93)90114-H
- M. A. Wieczorek, B. P. Weiss, S. T. Stewart, An impactor origin for lunar magnetic anomalies. *Science* **335**, 1212 (2012). doi:10.1126/science.1214773
[Medline](#)
- M. E. Purucker, J. B. Nicholas, Global spherical harmonic models of the internal magnetic field of the Moon based on sequential and coestimation approaches. *J. Geophys. Res.* **115**, E12007 (2010). doi:10.1029/2010JE003650
- D. E. Smith *et al.*, Initial observations from the Lunar Orbiter Laser Altimeter (LOLA). *Geophys. Res. Lett.* **37**, L18204 (2010). doi:10.1029/2010GL043751
- A. M. Rubin, Dike-induced faulting and graben subsidence in volcanic rift zones. *J. Geophys. Res.* **97**, 1839 (1992). doi:10.1029/91JB02170
- J. C. Andrews-Hanna, The origin of the non-mare mascon gravity anomalies in lunar basins. *Icarus* **10.1016/j.icarus.2012.10.031** (2012).
- G. A. Snyder, C. R. Neal, L. A. Taylor, A. N. Halliday, Processes involved in the formation of magnesian-suite plutonic rocks from the highlands of the Earth’s Moon. *J. Geophys. Res.* **100**, 9365 (1995). doi:10.1029/95JE00575
- E. M. Anderson, The Dynamics of Faulting and Dyke Formation with Application to Britain (Oliver and Boyd, London, ed. 2, 1951).
- S. C. Solomon, The relationship between crustal tectonics and internal evolution in the Moon and Mercury. *Phys. Earth Planet. Inter.* **15**, 135 (1977). doi:10.1016/0031-9201(77)90026-7
- H. J. Melosh, Tectonic patterns on a tidally distorted planet. *Icarus* **43**, 334 (1980). doi:10.1016/0019-1035(80)90178-5
- W. M. Kaula, Thermal evolution of Earth and Moon growing by planetesimal impacts. *J. Geophys. Res.* **84**, 999 (1979). doi:10.1029/JB084iB03p00999
- M. A. Wieczorek, R. J. Phillips, Potential anomalies on a sphere: Applications to the thickness of the lunar crust. *J. Geophys. Res.* **103**, 1715 (1998). doi:10.1029/97JE03136
- G. B. Reed, “Application of kinematical geodesy for determining short wave length components of the gravity field by satellite gradiometry” (Technical Report no. 201, Department of Geodetic Science, The Ohio State University, Columbus, OH, 1973).
- L. B. Pedersen, T. M. Rasmussen, The gradient tensor of potential field anomalies: Some implications on data collection and data processing of maps. *Geophysics* **55**, 1558 (1990). doi:10.1190/1.1442807
- L. Cordell, Gravimetric expression of graben faulting in Santa Fe Country and the Espanola Basin, New Mexico, *New Mexico Geol. Soc. Guidebook*, 30th Field Conf., pp. 59–64 (1979).

35. R. J. Blakely, *Potential Theory in Gravity and Magnetic Applications* (Cambridge Univ. Press, Cambridge, 1995).
36. N. Metropolis, A. W. Rosenbluth, M. N. Rosenbluth, A. H. Teller, E. Teller, Equations of state calculations by fast computing machine. *J. Chem. Phys.* **21**, 1087 (1953). [doi:10.1063/1.1699114](https://doi.org/10.1063/1.1699114)
37. D. L. Turcotte, G. Schubert, in *Geodynamics* (Cambridge Univ. Press, Cambridge, ed. 2, 2001), p. 528.
38. M. A. Kreslavsky, J. W. Head III, New observational evidence of global seismic effects of basin-forming impacts on the Moon from Lunar Reconnaissance Orbiter Lunar Orbiter Laser Altimeter data. *J. Geophys. Res.* **117**, E00H24 (2012). [doi:10.1029/2011JE003975](https://doi.org/10.1029/2011JE003975)
39. P. G. Lucey, D. T. Blewett, B. R. Hawke, Mapping the FeO and TiO₂ content of the lunar surface with multispectral imagery. *J. Geophys. Res.* **103**, 3679 (1998). [doi:10.1029/97JE03019](https://doi.org/10.1029/97JE03019)
40. D. J. Lawrence *et al.*, Global elemental maps of the moon: The Lunar Prospector gamma-ray spectrometer. *Science* **281**, 1484 (1998). [doi:10.1126/science.281.5382.1484](https://doi.org/10.1126/science.281.5382.1484) [Medline](#)
41. F. Nimmo, Dike intrusion as a possible cause of linear martian magnetic anomalies. *Geology* **28**, 391 (2000). [doi:10.1130/0091-7613\(2000\)28<391:DIAAPC>2.0.CO;2](https://doi.org/10.1130/0091-7613(2000)28<391:DIAAPC>2.0.CO;2)
42. C. M. Pieters, J. W. Head III, L. Gaddis, B. L. Jolliff, M. Duke, Rock types of South Pole-Aitken basin and extent of basaltic volcanism. *J. Geophys. Res.* **106**, 28001 (2001). [doi:10.1029/2000JE001414](https://doi.org/10.1029/2000JE001414)
43. H. Hiesinger, R. Jaumann, G. Neukum, J. W. Head III, Ages of mare basalts on the lunar nearside. *J. Geophys. Res.* **105**, 29239 (2000). [doi:10.1029/2000JE001244](https://doi.org/10.1029/2000JE001244)
44. L. Wilson, J. W. Head III, Tharsis-radial graben systems as the surface manifestation of plume-related dike intrusion complexes: Models and implications. *J. Geophys. Res.* **107**, 5057 (2002). [doi:10.1029/2001JE001593](https://doi.org/10.1029/2001JE001593)
45. L. L. Dimitrova, W. E. Holt, A. J. Haines, R. A. Schultz, Toward understanding the history and mechanisms of martian faulting: The contribution of gravitational potential energy. *Geophys. Res. Lett.* **33**, L08202 (2006). [doi:10.1029/2005GL025307](https://doi.org/10.1029/2005GL025307)
46. I. Matsuyama, F. Nimmo, Gravity and tectonic patterns of Mercury: Effect of tidal deformation, spin-orbit resonance, nonzero eccentricity, despinning, and reorientation. *J. Geophys. Res.* **114**, E01010 (2009). [doi:10.1029/2008JE003252](https://doi.org/10.1029/2008JE003252)
47. H. J. Melosh, Mascons and the Moon's orientation. *Earth Planet. Sci. Lett.* **25**, 322 (1975). [doi:10.1016/0012-821X\(75\)90248-4](https://doi.org/10.1016/0012-821X(75)90248-4)

Acknowledgments: The GRAIL mission is a component of the NASA Discovery Program and is performed under contract to the Massachusetts Institute of Technology and Jet Propulsion Laboratory. J.C.A.-H., J.W.H., W.S.K., I.M., P.J.M., F.N., and G.J.T. were supported by grants from the NASA GRAIL Guest Scientist Program. The data used in this study will have been archived in the Geosciences Node of the NASA Planetary Data System by the time of publication.

Supplementary Materials

www.sciencemag.org/cgi/content/full/science.1231753/DC1

Materials and Methods

Supplementary Text

Figs. S1 to S13

Tables S1 to S6

References (31–47)

19 October 2012; accepted 27 November 2012

Published online 5 December 2012

10.1126/science.1231753

Table 1. Density contrast ($\Delta\rho$), width (w), top depth (z_{top}), and bottom depth (z_{bot}) from the inversion of LGA-1, including the best-fit range in parameters and the 95% confidence intervals (C.I.) for the full inversion (7), and the best-fit ($\pm 95\%$ confidence interval range) solutions for assumed density contrasts of 550 and 800 kg m^{-3} .

	Best fit	95% C.I.	$\Delta\rho = 550$	$\Delta\rho = 800$
$\Delta\rho$ (kg m^{-3})	160–960	90–940	550	800
w (km)	4.5–24.9	5.7–46.7	$7.6^{+35.2}_{-1.4}$	$5.3^{+34.2}_{-0.9}$
z_{top} (km)	10.3–14.8	6.0–38.8	$13.0^{+28.2}_{-5.2}$	$13.3^{+30.0}_{-4.3}$
z_{bot} (km)	75.6–90.6	30–96	86^{+10}_{-55}	85^{+9}_{-56}

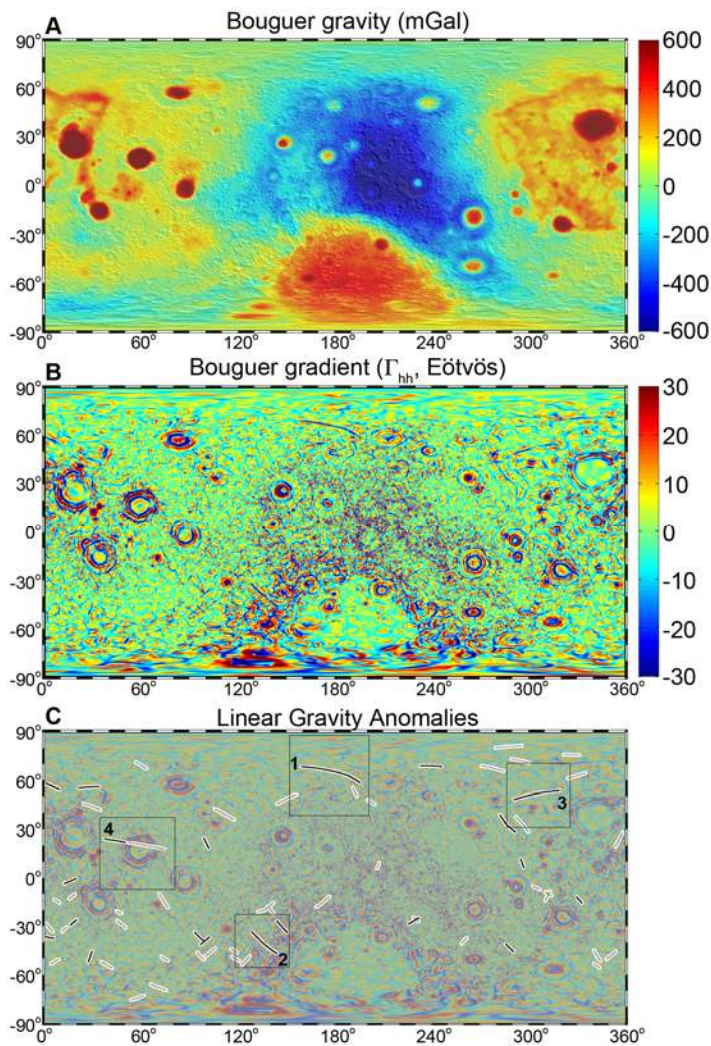


Fig. 1. (A) Bouguer gravity (from model GL0420A expanded to degree and order 300, assuming a density of 2560 kg m^{-3}), (B) horizontal Bouguer gradient (in Eötvös; generated from spherical harmonic degrees 50-300), and (C) a global mapping of the linear gravity anomalies (overlain on a muted Bouguer gradient map). In (C) anomalies are classified as probable (black lines) or possible (gray lines) LGAs, as described in the text. The largest anomalies discussed herein are numbered 1-4. All panels are in a simple cylindrical projection, centered on the far side.

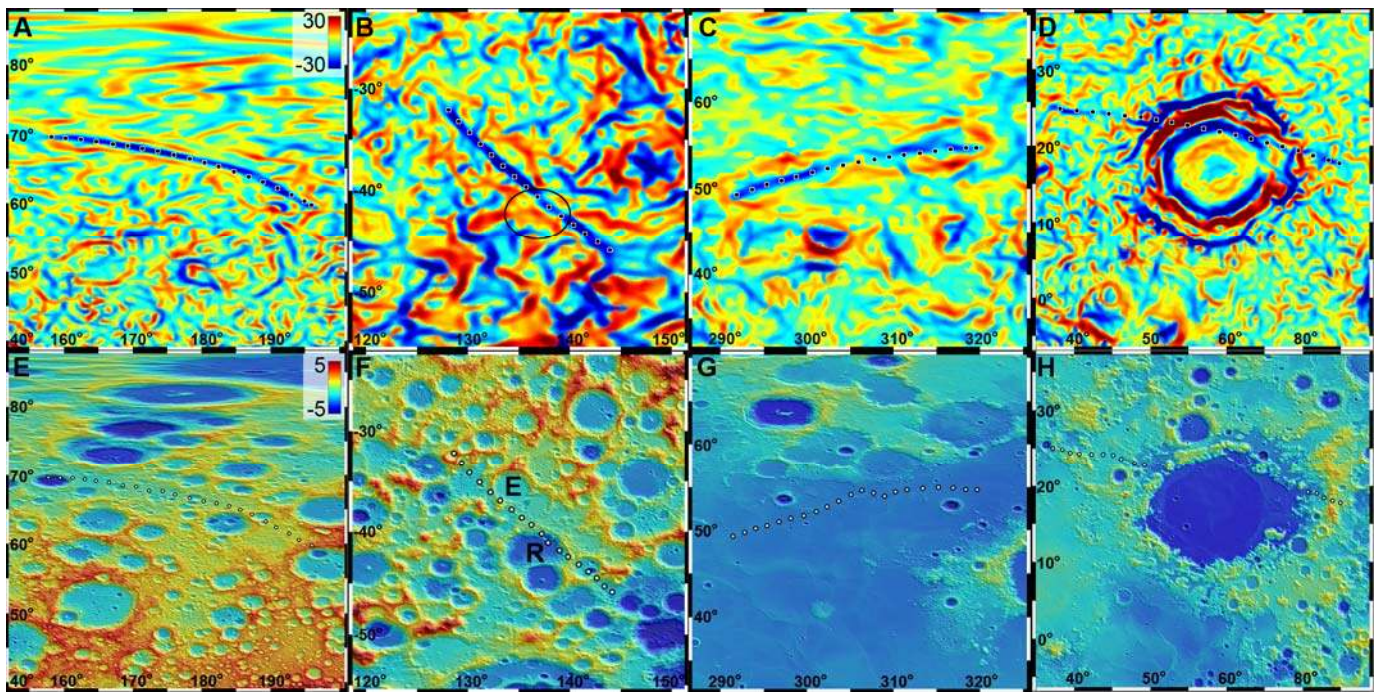


Fig. 2. (A to D) Horizontal Bouguer gradient (in Eötvös) and (E to H) topography (in km) in the vicinity of four prominent linear gravity anomalies (LGAs 1-4, left to right; see Fig. 1 for context). The dots in the upper panels follow great-circle fits to the anomalies, whereas the dots in the lower panels follow the paths of the anomalies themselves. The craters Eötvös (E) and Roche (R) are labeled in (F), and Roche is outlined in (B); the gravity gradient shows reduced amplitude within the latter crater.

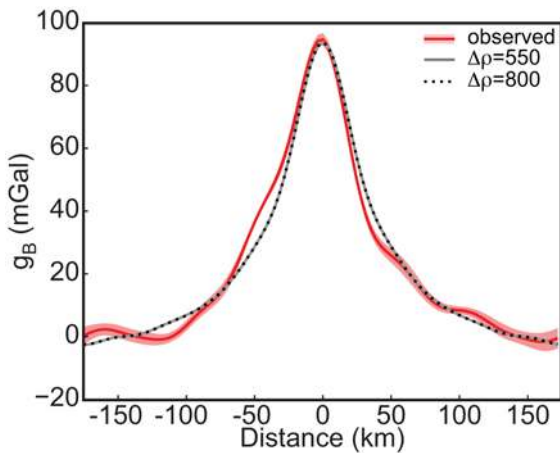


Fig. 3. Mean profile and ± 1 standard error range (in red and pink) of the Bouguer gravity anomaly over LGA-1. The predicted gravity from the best-fit vertical tabular intrusions for density contrasts of 550 and 800 kg m^{-3} are shown for comparison (overlapping gray and dashed black lines).